

An improved method for the theoretical prediction of the wave resistance of transom-stern hulls using a slender body approach

Mr P.R. Couser, Dr J.F. Wellicome and Dr A.F. Molland

*Department of Ship Science
University of Southampton, U.K.*

An existing numerical method for calculating the wave pattern and hence wave resistance of a body moving in a free surface has been improved and developed. A potential, non-lifting, model has been used with linearised free surface conditions to describe the flow around a body in a finite channel. The model has been developed specifically for calculating the wave pattern resistance of slender catamaran hulls with transom sterns, but may be applied to more general ship hull-forms provided that they have sufficiently high Length: Breadth ratio. The bodies are represented by planar arrays of sources on the local hull centre-lines. Particular attention has been made to the closure of the model in the region of the transom stern and results have been compared with experimental measurements carried out by the authors. Comparisons have also been made with results obtained from higher-order panel codes. Good correlation with both experiment and higher-order methods have been found for the slender hull forms investigated. The method presented offers orders of magnitude saving in computational effort over the higher-order methods without sacrificing accuracy.

1 Introduction

The application of linear, slender body, numerical models to the wave resistance problem is wide spread since these methods can provide fast, accurate solutions for slender hull types. Developments to the original methods of researchers such as Mitchell[1], Wigley[2] and Eggers[3] have been made, and this method can now be applied to a wide range of hull forms. For example Insel[4, 5], Cong and Hsiung[6], Yim[7], etc. The work described here uses the method developed by Insel[4] where the wave resistance is calculated from the description of the far-field wave system using Eggers coefficients.

Although this method has been successfully applied to simple hull forms such as the Wigley hull, problems have been encountered when applying such methods to transom-stern hulls. Several alternatives have been put forward. Here a comparison of several approaches for modelling the

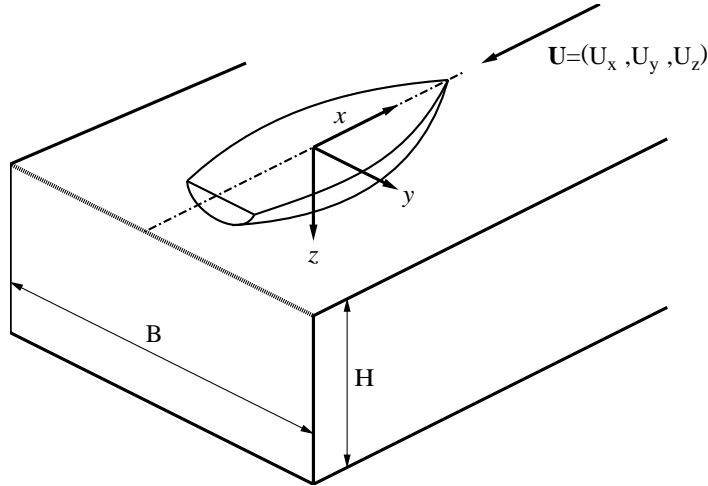


Figure 1: Main notation and axis convention

transom is made; a new method which involves the addition of a ‘virtual appendage’ aft of the transom is described.

2 Summary of existing theory

The slender body approach is numerically less computationally intensive than linear panel methods and many times faster than the non-linear solutions. A typical linear panel method will take 400 – 500 CPU seconds, on a Sun IPX workstation, to calculate the resistance at one speed. This can be multiplied by a factor of 4 – 10 for the non-linear solution depending on the number of iterations required for convergence. A whole range of speeds can be calculated using the slender body approximation in a fraction of this time.

The main disadvantage of using a slender body approximation occurs for wide beam hulls near the limit of the slender body assumption. However, the catamaran hulls of interest in this investigation are generally very slender, with Length: Breadth ratios of the order of 10 – 15.

A major disadvantage of using a linear panel method can occur if the resistance is calculated from pressure integration. If a substantial bow wave exists a large error in resistance may be found. Similarly an over estimate in the stern wave amplitude can result in negative wave resistance being predicted, especially for canoe stern hulls at slow speeds. However with the slender body method the resistance is calculated from the far-field wave system and is thus not so susceptible to these sorts of problems.

2.1 The existing slender body model formulation

The existing slender body method was developed by Insel[4] and has formed the basis from which the current work stems. Figure 1 shows the axis system used. The hull is in a finite channel of water depth H , and width B . The positive x , y and z axes are in the forward, starboard and downwards directions respectively; with the tank centreline at $y = 0$ and the undisturbed free-surface at $z = 0$.

The hull is discretised into a large number of quadrilateral panels. Source singularities are then placed adjacent to each panel centre on the $y = 0$ plane to form an array along the centreline of the hull. The source strengths are calculated independently of each other and depend only on

the local panel slope. In the original formulation the source strength, on a panel of the hull, is proportional to the waterline slope, Equation 1.

$$\sigma = \frac{U_x}{2\pi} \frac{dy}{dx} \times \text{projected panel area on the } y = 0 \text{ plane} \quad (1)$$

where $\frac{dy}{dx}$ is the waterline slope and U_x is the onset free stream, which will be negative.

In the current work Equation 1 is re-arranged to provide a more flexible expression for the source strength which is now calculated from the panel normal, Equation 2

$$\sigma = \frac{-1}{2\pi} \hat{\mathbf{n}} \cdot \mathbf{U} \times \text{panel area} \quad (2)$$

where $\hat{\mathbf{n}}$ is the outward unit normal vector of the panel and $\mathbf{U} = (U_x, U_y, U_z)$ is the onset free stream.

The advantage of Equation 2 over Equation 1 is that the source strength is always defined even where the waterline slope $\left(\frac{dy}{dx}\right)$ tends to infinity and the projected area tends to zero; for example on the transom.

Multi-hull vessels can be represented by a number of source arrays, one for each hull, placed at the required positions in the channel.

The wave resistance of the sources is calculated from an expression derived by Insel[4] which describes the resistance in terms of far-field Eggers coefficients[3] for a source in a finite channel, Equation 3. The resistance of the sources is dependent on the wave harmonic, m ; to obtain the total wave pattern resistance approximately 100 – 150 harmonics are used.

$$R_{WP} = \frac{\rho g B}{4} \left\{ \zeta_0^2 \left[1 - \frac{2k_0 H}{\sinh(2k_0 H)} \right] + \sum_{m=1}^{\infty} \zeta_m^2 \left[1 - \frac{\cos^2 \theta_m}{2} \left(1 + \frac{2k_m H}{\sinh(2k_m H)} \right) \right] \right\} \quad (3)$$

where the wave elevation for a given harmonic ζ_m is given by Equation 4:

$$\zeta_m^2 = \xi_m^2 + \eta_m^2 \quad (4)$$

and the elevation terms for a source at $(x_\sigma, y_\sigma, z_\sigma)$ are given by Equation 5:

$$\begin{aligned} \left| \begin{array}{c} \xi_m \\ \eta_m \end{array} \right| &= \frac{16\pi U}{Bg} \frac{\bar{k} + k_m \cos^2 \theta_m}{1 + \sin^2 \theta_m - \bar{k} H \operatorname{sech}^2(k_m H)} \\ &\sum_{\sigma} \left[\sigma_{\sigma} e^{-k_m H} \cosh[k_m(H + z_{\sigma})] \left| \begin{array}{c} \cos(k_m x_{\sigma} \cos \theta_m) \\ \sin(k_m x_{\sigma} \cos \theta_m) \end{array} \right| \left\{ \begin{array}{c} \cos \frac{m\pi y_{\sigma}}{B} \\ \sin \frac{m\pi y_{\sigma}}{B} \end{array} \right\} \right] \end{aligned} \quad (5)$$

Noting that the term for $m = 0$ is halved and that the last cosine term applies to even m and the sine term to odd m . The summation represents the effect of all the sources describing the hull, typically 800.

The fundamental wave number is given by: $\bar{k} = g/U^2$. Also the wave number k_m and the wave angle θ_m of the m th harmonic satisfy the wave speed condition, including shallow water effects, (Equation 6) and the wall reflection condition (Equation 7), noting that $\bar{k} = k_0$ if deep water is assumed.

$$k_m - \bar{k} \sec^2 \theta \tanh(k_m H) = 0 \quad (6)$$

$$k_m \sin \theta_m = \frac{m\pi}{B} \quad (7)$$

Although this method has been successfully applied to simple hullforms such as the Wigley hull, problems have been encountered when applying such methods to high-speed, transom-stern hulls. Several modifications to the original theory have been made and they are examined below.

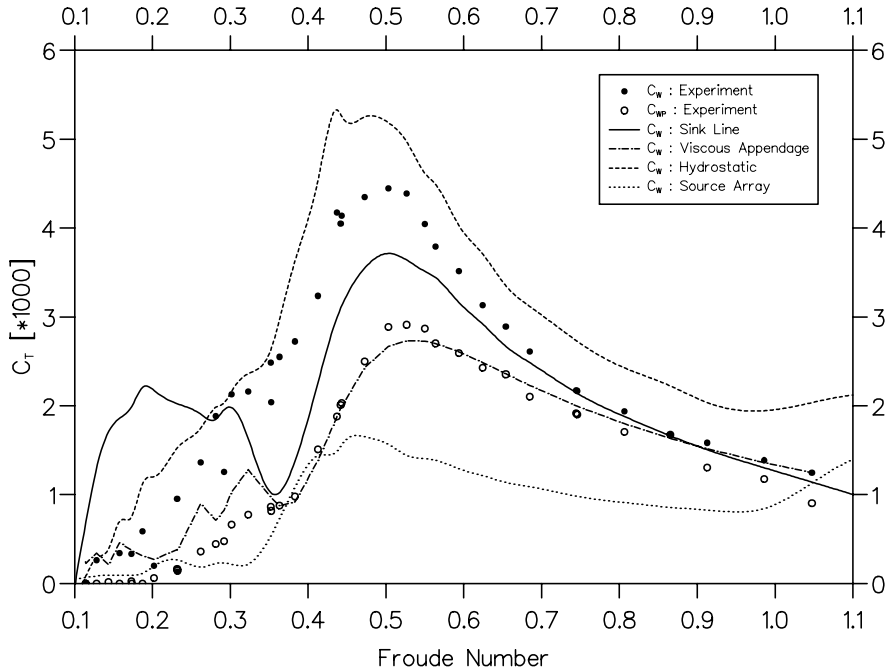


Figure 2: Wave resistance calculations: Model 4a Monohull

3 Modifications to existing theory

3.1 Trim and sinkage

An estimate of the running waterline was made by sinking and trimming the hull by the values measured during the experimental programme[8, 9]. However the actual wave profile along the side of the hull was not taken into account. Due to the slender nature of the hulls in question and the relatively small changes in running trim and sinkage, the waterline slopes did not change significantly at running attitude when compared with the static case. This was reflected in relatively small differences between the basic source array wave resistance for the two attitudes. However, the effect of two degrees of trim over the hull length significantly increased the immersed transom depth and area. This change in immersed transom area had far greater effect on the resistance prediction than the change in waterline slope due to trim and sinkage. As has been mentioned earlier, resistance is calculated from the far-field wave system and *not* from a pressure integration over the hull. Thus this relatively simple method for estimating the underwater portion of the hull is valid.

3.2 Transom stern effects

Most slender body methods omit sources on the transom. This is due to the fact that the waterline slope $\frac{dy}{dx}$ in Equation 1 is undefined on the transom. (It should be noted that the use of Equation 2 alleviates this problem.) If the model is not closed at the stern by the use of Equation 2 there is a source deficit which causes the resistance to be under predicted when compared with experimental measurements of wave pattern resistance. Several methods for making up this resistance deficit have been developed by various researchers, including a hydrostatic correction, a transom source correction and a new virtual appendage approach proposed in this paper. Results of calculations using the various transom stern models have been compared with experimental results of C_{WP} and C_W for monohull Model 4a and are presented in Figure 2. Details of the models used in the experimental programme and referenced to in this paper are given in Table 1. The model

Table 1: Details of the Models

| Model | L [m] | L/B | B/T | $L/\nabla^{\frac{1}{3}}$ | C_B | C_P | C_M | A [m ²] | LCB |
|-------|---------|-------|-------|--------------------------|-------|-------|-------|-----------------------|------|
| 4a | 1.6 | 10.4 | 1.5 | 7.40 | 0.397 | 0.693 | 0.565 | 0.348 | -6.4 |
| 5c | 1.6 | 9.9 | 2.5 | 8.49 | 0.397 | 0.693 | 0.565 | 0.277 | -6.4 |
| 6b | 1.6 | 13.1 | 2.0 | 9.50 | 0.397 | 0.693 | 0.565 | 0.233 | -6.4 |

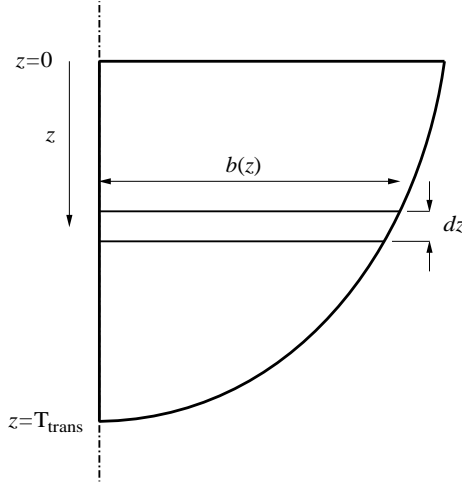


Figure 3: Hydrostatic transom correction

notation is that used in Refs.[8, 9]. In Figure 2, the conventional estimate of wave resistance $C_W = C_T - (1 + k)C_F$ is denoted by the solid dots and the measured wave pattern resistance C_{WP} by the open dots. The resistance of the source array with no transom correction is seen to be very much less than the experimental results. Both the hydrostatic correction and the sink line correction over estimate C_{WP} . The virtual appendage correction gives excellent correlation with C_{WP} .

It should be noted that C_{WP} is calculated from experimental measurements of the far-field wave system and analysis using potential theory. Hence it can be argued that the results from the slender body model, which are also calculated from the far-field, should be compared with C_{WP} and not C_W . From a practical point of view it is useful to calculate C_W since total resistance, $C_T = (1 + k)C_F + C_W$, can then be simply calculated from C_W provided the form factor is known. (Both C_{WP} — open dots, and C_W — solid dots are presented in Figure 2.)

The formulations of the various transom corrections mentioned above are now discussed in greater depth:

3.2.1 Hydrostatic correction

A hydrostatic transom correction can be applied to the drag of the source array to produce the total wave resistance. The transom resistance is calculated by integrating the static pressure acting on the transom (Equation 8).

$$R_{\text{trans}} = \rho g \int_0^{T_{\text{trans}}} z.b(z) dz \quad (8)$$

where T_{trans} is the transom draught and $b(z)$ defines the transom half-beam at depth z , see Figure 3.

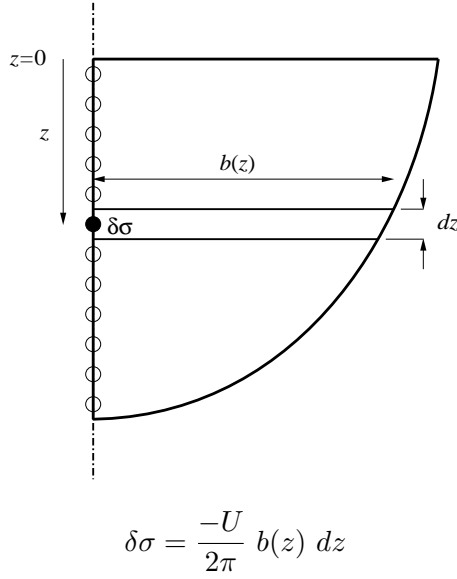


Figure 4: Source distribution for closed transom method

This method is valid for speeds at which the transom is running clear ($Fn > 0.5$) and is relatively successful especially at these higher speeds. However since the correction is only dependent on transom area and not on speed, the effect of dividing by U^2 as the velocity tends to zero produces a coefficient which increases dramatically at lower speeds. In the presented form the hydrostatic correction has been linearly reduced from its full value at $Fn = 0.5$ to zero at $Fn = 0.1$. It can be seen that although this method gives a reasonable approximation to the shape of the C_W resistance curve there is a 30% – 40% increase in magnitude over the entire speed range. This method yields even worse predictions of C_{WP} , especially at low to moderate Froude number.

3.2.2 Closed transom and sink line

Here sources are placed in various configurations over the transom.

The first method involves closing the transom with centre-line sources calculated according to Equation 2 with $\hat{n} = (-1, 0, 0)$ and $\mathbf{U} = (U_x, 0, 0)$ (Noting that U_x will be negative), see Figure 4.

The second involves placing sinks along a transverse sink line across the bottom of the transom, similar to that used by Yim[7] and Cong and Hsiung[6].

$$\delta\sigma(-L/2, \pm b, z(b)) = \frac{-U}{4\pi} z(b) db \quad (9)$$

Two sources of strength $\delta\sigma$, given by Equation 9, are placed at the longitudinal position of the transom ($x = -L/2$), either side of the centre plane ($y = \pm b$), and at a depth corresponding to the transom depth $z(b)$ at $y = b$. The source distribution for the sink line method is shown in Figure 5

Both methods give the same total source strength over the transom but with different singularity positions. As may be expected, both methods yield similar results and the curve for the sink line method is shown by the full line in Figure 2. As can be seen, results at speeds above moderate Froude number ($Fn > 0.35$) are reasonable, lying somewhere between the two sets of experimental results; whilst the model is rather poor below this speed.

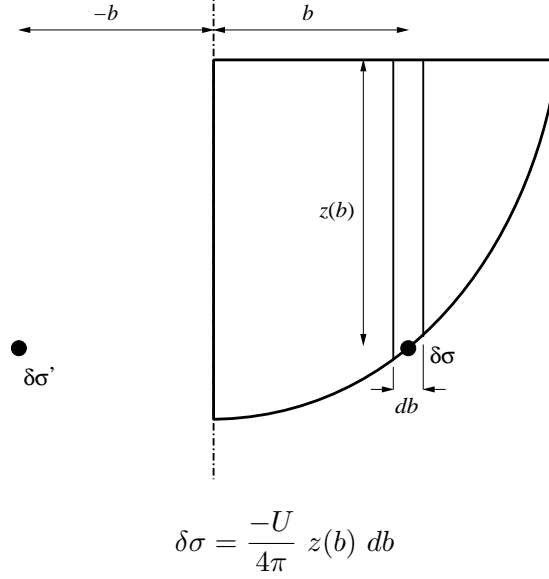


Figure 5: Source distribution for closed transom method

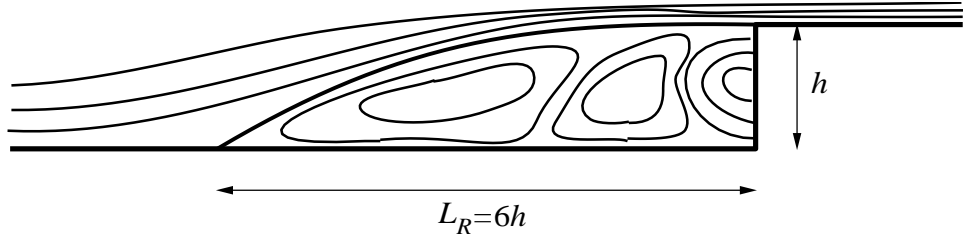


Figure 6: Flow over a backward facing step

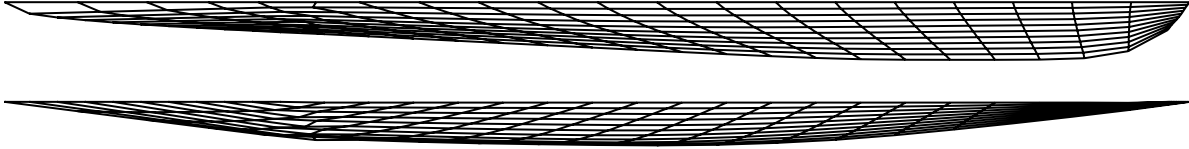
3.2.3 Virtual appendage

This method involves the addition of a virtual appendage to the transom which encloses the separated flow in the low speed range and the air pocket in the high speed range.

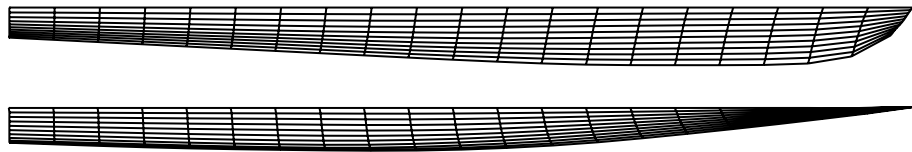
The horizontal planar flow around the transom may be considered by examining the two dimensional flow over a backward facing step (see Figure 6). It is noted by Batchelor[10] and Sinha[11] that the streamline re-attachment length behind the step tends to six times the step height for high Reynolds number turbulent flow. In this manner the transom stern body is closed by the addition of an extra point down stream of the transom for each water line; the down stream offset being six times the transom half breadth (see Figure 7).

The virtual appendage correction in Figure 2 gives excellent correlation with C_{WP} . A fixed re-attachment length of six times the transom half-breadth was used for this calculation. However, it is possible to optimise the predictions by varying the re-attachment length slightly. The variation in re-attachment length shown in Figure 8 was used for the rest of the calculations presented. This variation was obtained by running the model with various constant re-attachment lengths and then choosing the re-attachment length which gave best results over a specific Froude number range.

It has been already mentioned that, for design purposes, it is more useful to be able to estimate C_W since then only $(1+k)C_F$ need be evaluated to obtain C_T . The virtual appendage model gives good agreement with C_{WP} and the deficit between the two can be made up either by regression analysis of the difference between C_{WP} and C_W and incorporating a multiplication factor, or by investigating the physical processes causing the difference and developing numerical



Virtual appendage added down stream of transom (20x10 mesh)



No virtual appendage (20x10 mesh)

Figure 7: Hull discretisation with and without virtual appendage

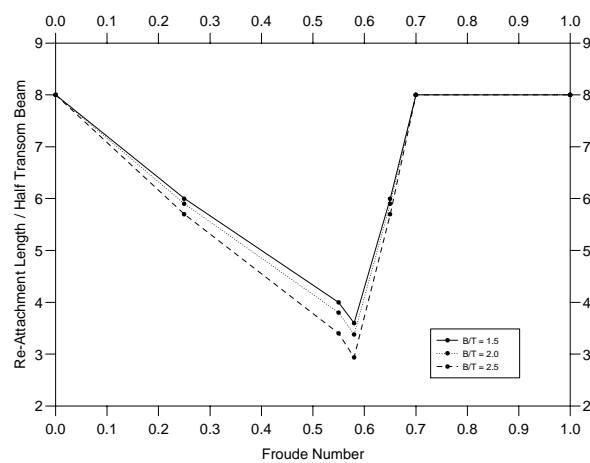


Figure 8: Variation in re-attachment length with F_n and B/T

tools for estimating these components. A regression analysis method has shown promising results but may limit the application of the results to one type of hullform.

4 Comparison of modified theory with experiment

In comparing the results from theoretical predictions with experimental results it should be noted that the slender body method models the far field potential flow around a streamlined body. Thus it would be expected that the theory should match the experimental measurements of wave pattern resistance (C_{WP}) which were derived from measurements of the far field wave system. Figure 2 compared the effectiveness of the various transom models at predicting the wave pattern resistance. It can be seen that the virtual appendage model provided good agreement over most of the speed range. It is perhaps surprising that this method is effective even in the region before the transom is running clear. In this flow regime the virtual appendage encloses the stagnated flow behind the hull(s). The other methods were found to over-predict the wave pattern resistance, especially the hydrostatic correction.

Since the virtual appendage model appeared to be most effective at modelling the physical processes generating wave pattern resistance, this method was used to calculate the wave pattern resistance of all the models tested and excellent correlation between calculated and measured wave pattern resistance was found in every case. Some results of the calculations using the virtual appendage model are presented in Figures 9 to 23, where theoretical calculations are compared with the experimental measurements of C_{WP} from the far field wave pattern analysis. It was found that best results were obtained if the re-attachment length of the virtual appendage was varied with Froude number. This was done in an arbitrary manner and the physical implications of this have yet to be fully investigated. The variation of re-attachment length with Froude number is given in Figure 8; the growth from the transom transition ($F_n = 0.45$) with increasing speed reflects the physical observations made during the tank tests. The growth as the Froude number is decreased from the transition is more difficult to justify since the region of stagnated flow is not easily observed during testing.

The effect of panel distribution was investigated for one model at one Froude number, and the results are presented in Figure 24. For the calculations of C_{WP} presented here, a distribution of 40 longitudinal x 20 transverse panels was used. This panel distribution offered good accuracy in a reasonable computational time.

Typical free surface elevations have been calculated for one monohull, and one catamaran configuration, Figures 25 and 26. For the far-field wave pattern, calculation of the free-surface elevation is straight forward, since the amplitudes of all the wave harmonics are known, and may be useful for investigating the size of the wash created.

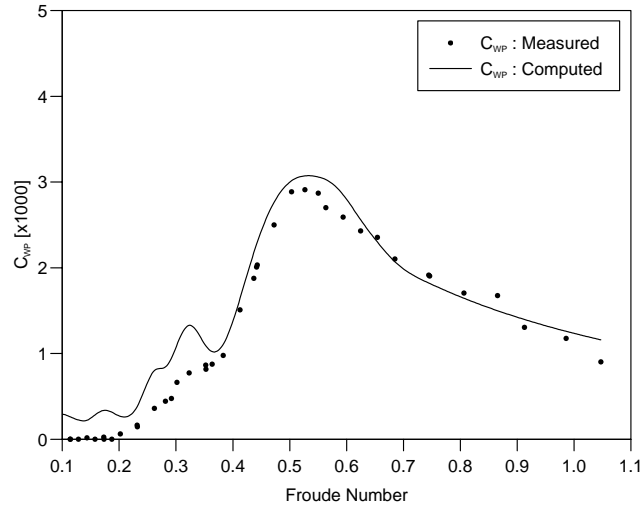


Figure 9: Results from Virtual Appendage model — 4a Monohull

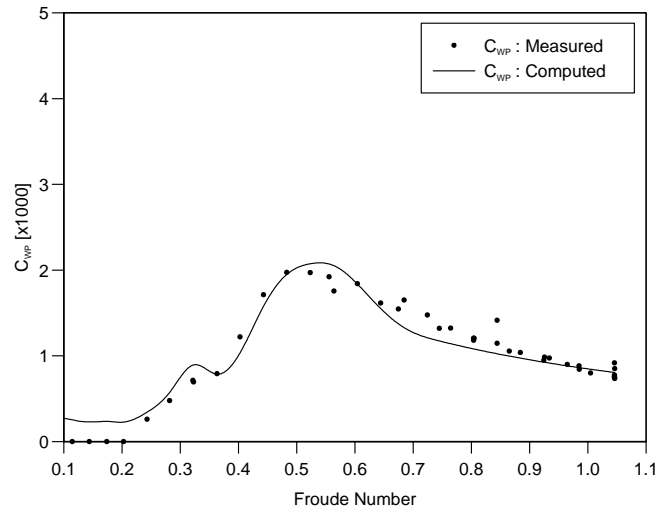


Figure 10: Results from Virtual Appendage model — 5c Monohull

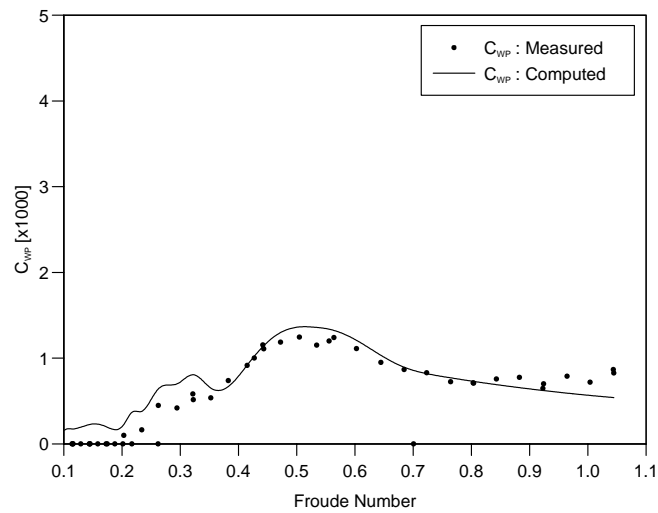


Figure 11: Results from Virtual Appendage model — 6b Monohull

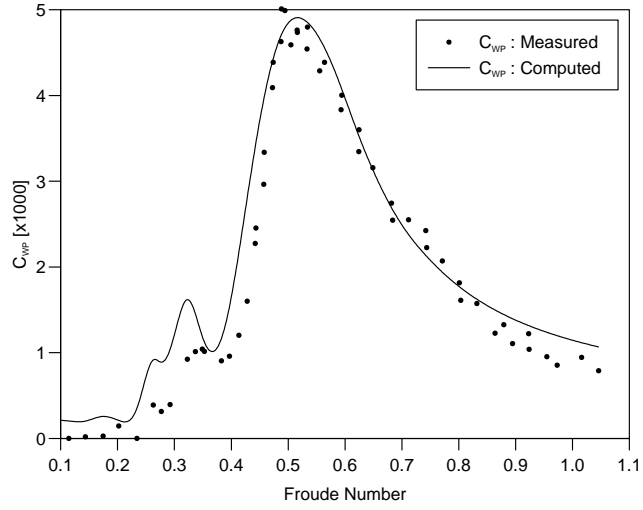


Figure 12: Results from Virtual Appendage model — 4a $S/L=0.2$

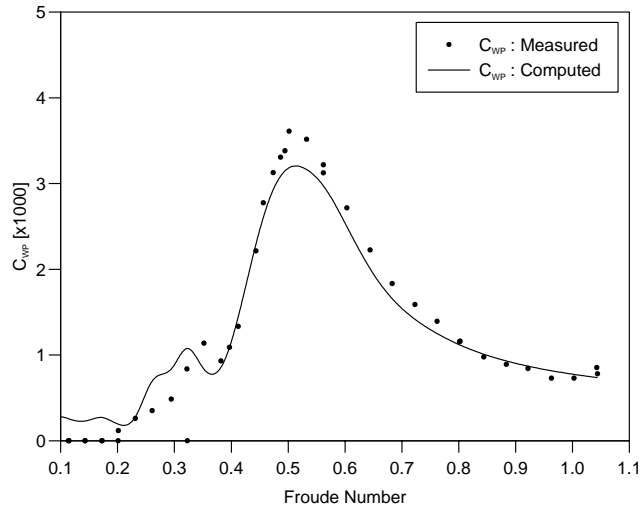


Figure 13: Results from Virtual Appendage model — 5c $S/L=0.2$

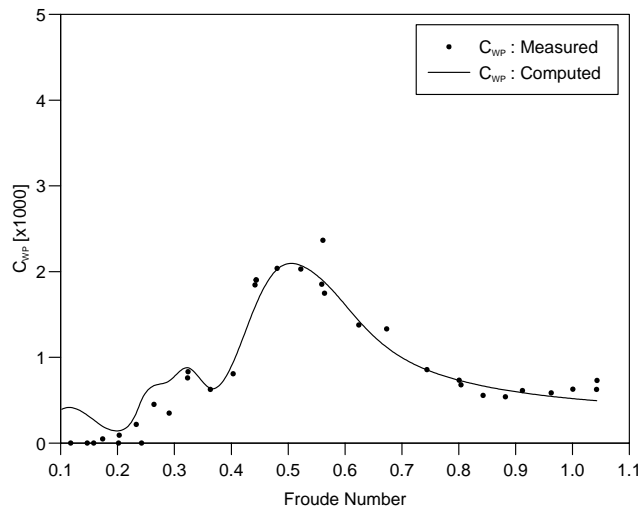


Figure 14: Results from Virtual Appendage model — 6b $S/L=0.2$

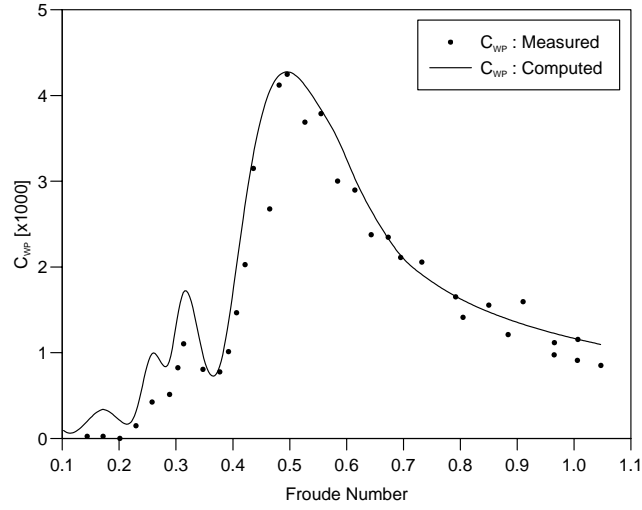


Figure 15: Results from Virtual Appendage model — 4a $S/L=0.3$

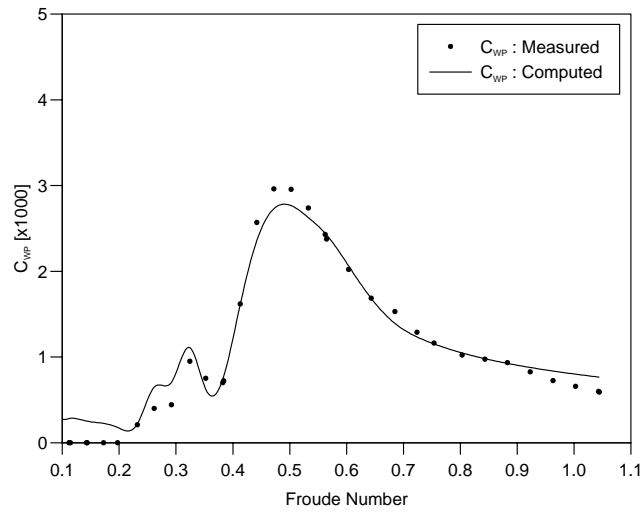


Figure 16: Results from Virtual Appendage model — 5c $S/L=0.3$

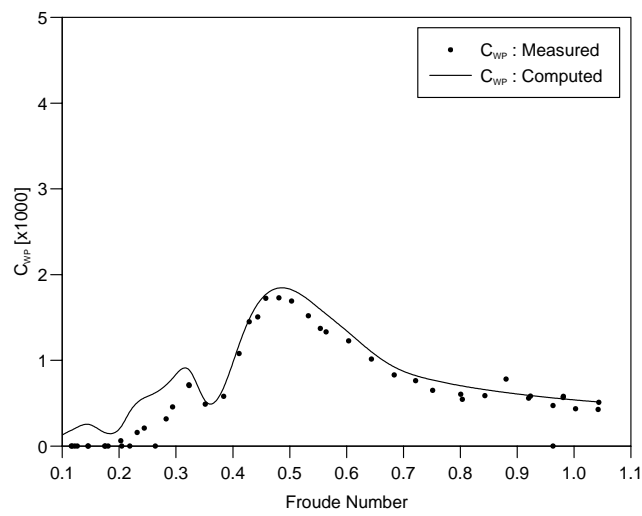


Figure 17: Results from Virtual Appendage model — 6b $S/L=0.3$

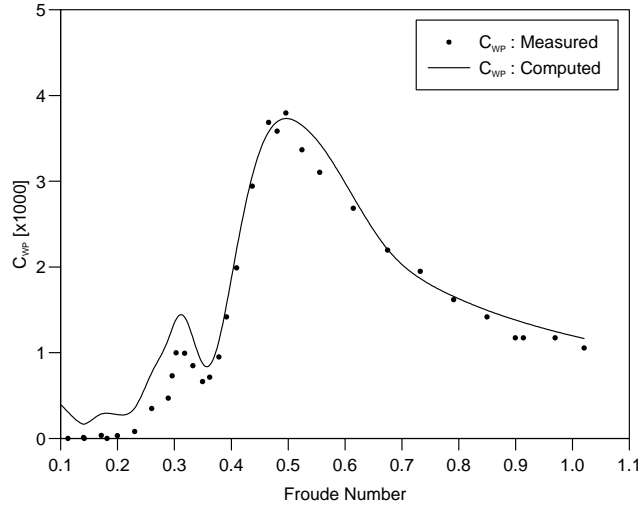


Figure 18: Results from Virtual Appendage model — 4a $S/L=0.4$

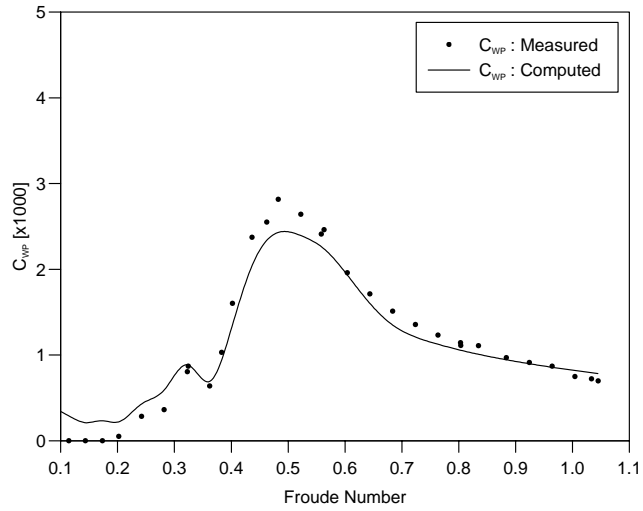


Figure 19: Results from Virtual Appendage model — 5c $S/L=0.4$

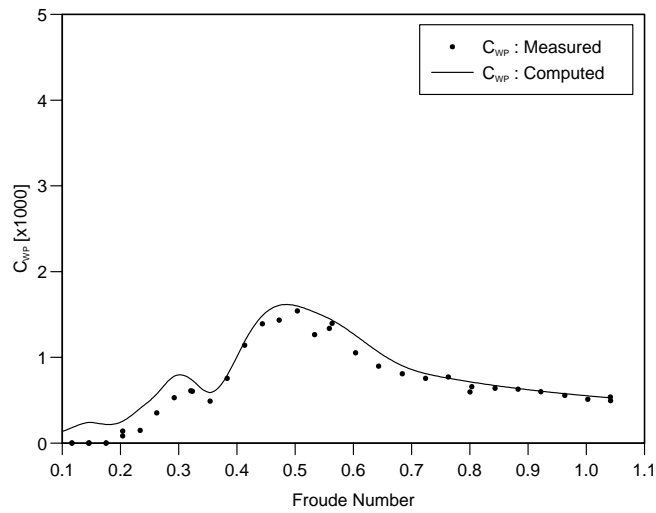


Figure 20: Results from Virtual Appendage model — 6b $S/L=0.4$

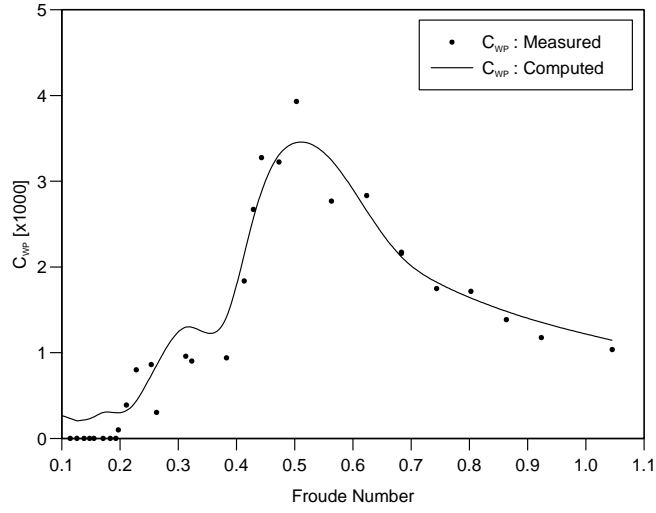


Figure 21: Results from Virtual Appendage model — 4a $S/L=0.5$

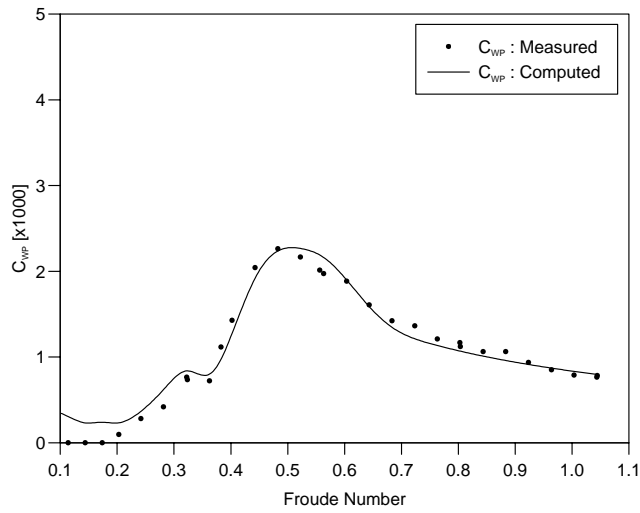


Figure 22: Results from Virtual Appendage model — 5c $S/L=0.5$

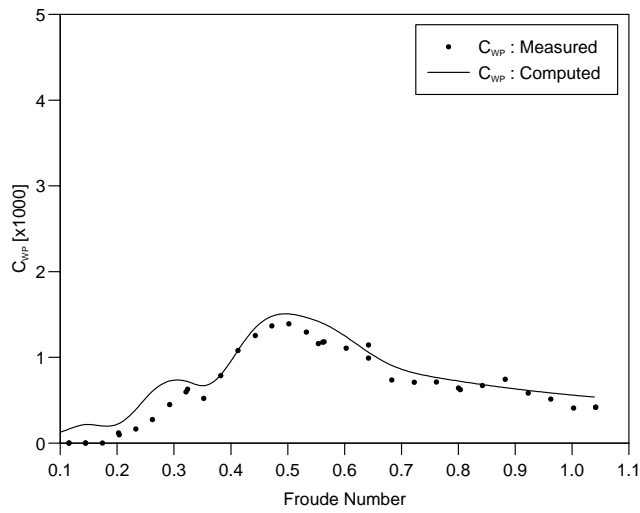


Figure 23: Results from Virtual Appendage model — 6b $S/L=0.5$

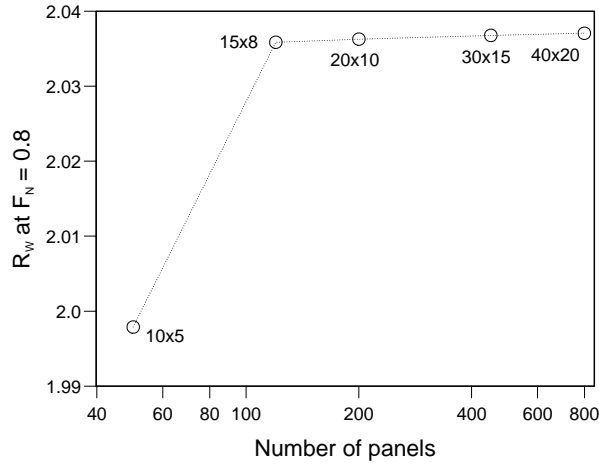


Figure 24: Effect of panel density on R_w

5 Conclusions

A new method for applying slender body calculations to transom-stern multihull vessels has been described. This method has been shown to provide excellent predictions of wave pattern resistance for catamarans and monohulls with a variety of geometries. The main findings are summarised as follows:

- Improvements in the prediction capabilities of the original slender body theory have been achieved. The modifications to include experimentally measured running trim and sinkage have been beneficial to the analysis.
- The virtual appendage model for the transom correction gives good results for wave pattern resistance and warrants further developments so that it may be used to provide a practical estimate of wave resistance. Results using the modified slender body method produce results comparable with those of higher order methods for these types of slender hulls, and orders of magnitude savings can be made in the time and computing resources required.
- Overall, the slender body method with a virtual appendage transom correction offers the ability to make very realistic estimates of catamaran wave pattern resistance over most of the speed range, and provides a very useful practical design tool for parametric studies.

6 Nomenclature

| | |
|-----------|---|
| B | Tank width, Demihull maximum beam |
| b | Local beam |
| C_F | Coefficient of frictional resistance |
| C_T | Coefficient of total resistance |
| C_W | Conventional estimate of coefficient of wave resistance |
| C_{WP} | Coefficient of wave pattern resistance |
| F_n | Froude Number |
| g | Acceleration due to gravity |
| H | Tank depth |
| h | Step height |
| \bar{k} | Fundamental wave number |

| | |
|--------------------------------|---|
| k_m | Wave number of m th harmonic |
| $1 + k$ | Form factor |
| $L/\nabla^{\frac{1}{3}}$ | Length : displacement ratio |
| L | Demihull length between perpendiculars |
| L_R | Streamline re-attachment length |
| m | Harmonic number |
| \hat{n} | Outward panel normal |
| R_F | Friction resistance |
| R_T | Total resistance (to forward motion) |
| R_{trans} | Transom resistance correction |
| R_W | Conventional estimate of wave resistance |
| R_{WP} | Wave pattern resistance |
| S | Separation between catamaran demihull centrelines |
| T | Demihull draught |
| T_{trans} | Draught at stem |
| T_σ | Draught of source |
| U | Onset free stream |
| $x_\sigma, y_\sigma, z_\sigma$ | position of source |
| z | Local depth |
| θ_m | Wave angle of m th harmonic |
| ζ_m | Wave amplitude of m th harmonic |
| ξ_m | Even wave amplitude component of m th harmonic |
| η_m | Odd wave amplitude component of m th harmonic |
| ρ | Density |

References

- [1] J.H. Mitchell. The wave resistance of a ship. *Philosophical Magazine, London, Series 5*, 45(272):106–123, January 1898.
- [2] W.C.S. Wigley. A comparison of experimental and calculated wave-profiles and wave-resistances for a form having parabolic waterlines. *Royal Philosophical Society, London*, 144, March – May 1933.
- [3] K. Eggers. Resistance components of two-body ships. *Jahrbuch der Schiffbautechnischen Gesellschaft*, 49, 1955.
- [4] M. Insel. *An Investigation into the Resistance Components of High Speed Displacement Catamarans*. PhD thesis, University of Southampton, 1990.
- [5] M. Insel and A.F. Molland. An investigation into the resistance components of high speed displacement catamarans. *Transactions, Royal Institution of Naval Architects*, 1992.
- [6] L. Cong and C.C. Hsiung. A simple method of computing wave resistance, wave profile, and sinkage and trim of transom stern ships. *ITTC*, 1990.
- [7] B. Yim. Analyses of waves and the wave resistance due to transom-stern ships. *Journal of Ship Research*, June 1969.
- [8] A.F. Molland, J.F. Wellicome, and P.R. Couser. Resistance experiments on a systematic series of high speed displacement catamaran forms: Variation of length-displacement ratio and breadth-draught ratio. Ship Science Report 71, Department of Ship Science, University of Southampton, March 1994.

- [9] A.F. Molland, J.F. Wellicome, and P.R. Couser. Resistance experiments on a systematic series of high speed displacement catamaran forms: Variation of length-displacement ratio and breadth-draught ratio. *Paper presented to the Royal Institution of Naval Architects*, November 1995.
- [10] G.K. Batchelor. A proposal concerning wakes behind bluff bodies at large reynolds numbers. *Journal of Fluid Mechanics*, 6:547–567, November 1959.
- [11] S.N. Sinha. Backward facing step flow experiments. *AIAA Journal*, 19:1527–1530, 1981.

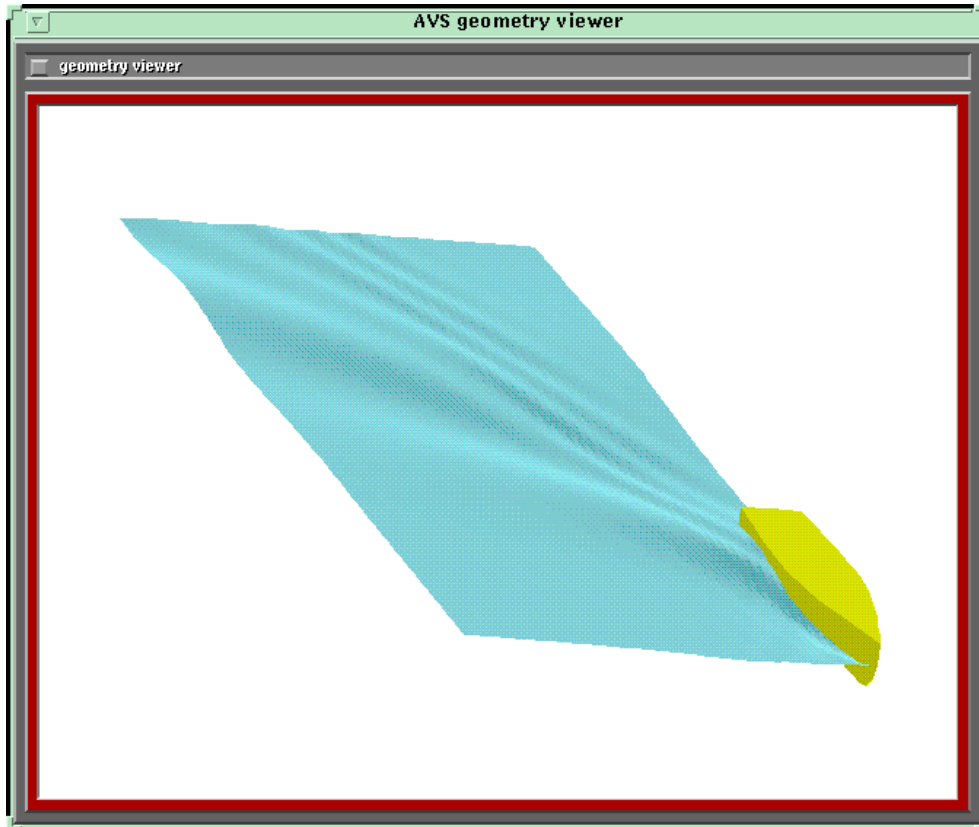


Figure 25: Free surface for 4b Monohull, $F_n = 0.5$

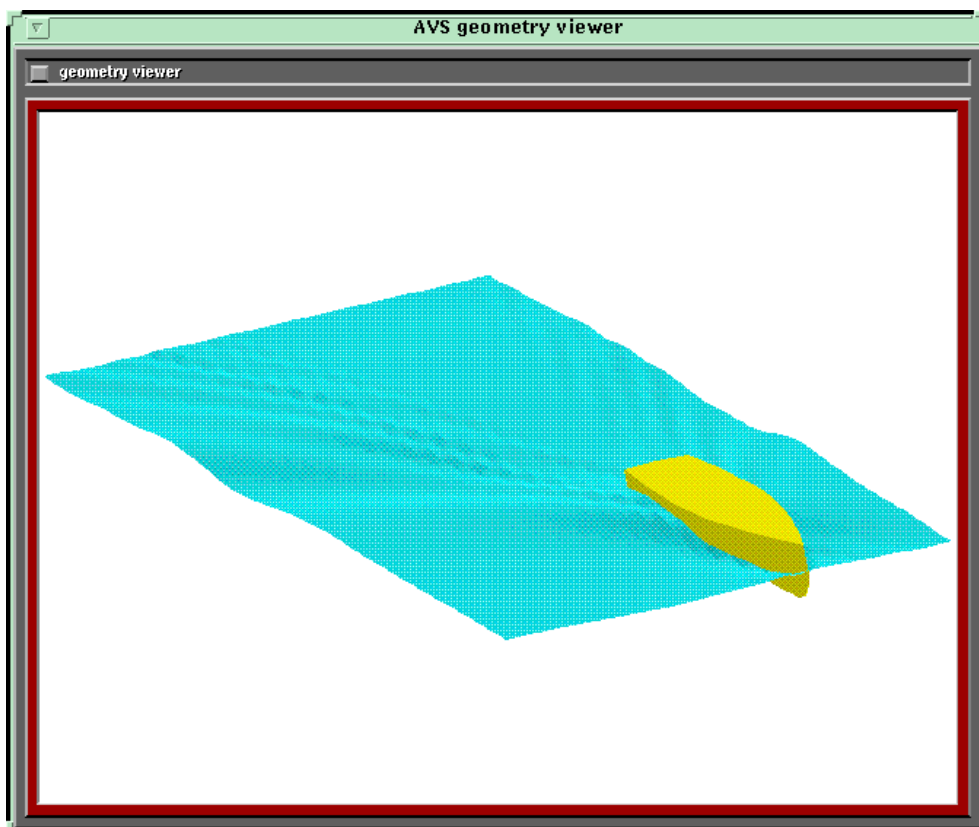


Figure 26: Free surface for 4b $S/L = 0.2$, $F_n = 0.5$